

## Evaluation of gamma-irradiation effects on the electrical properties of Al/(ZnO-PVA)/p-Si type Schottky diodes using current-voltage measurements

Ahmet Kaymaz<sup>a,\*</sup>, Esra Evcin Baydilli<sup>a</sup>, Habibe Uslu Tecimer<sup>b</sup>, Şemsettin Altindal<sup>c</sup>, Yashar Azizian-Kalandaragh<sup>d,e</sup>

<sup>a</sup> Electrical-Electronics Engineering Department, Karabuk University, Karabuk, Turkey

<sup>b</sup> Medical Engineering Department, Karabuk University, Karabuk, Turkey

<sup>c</sup> Department of Physics, Gazi University, Ankara, Turkey

<sup>d</sup> Department of Physics, University of Mohaghegh Ardabili, Ardabil, Iran

<sup>e</sup> Department of Engineering Sciences, Sabalan University of Advanced Technologies (SUAT), Namin, Iran



### ARTICLE INFO

**Keywords:**

Al/(ZnO-PVA)/p-Si type Schottky diodes  
Organic/polymer interlayer  
Gamma-irradiation effect  
Annealing effect  
Energy distribution of the surface states

### ABSTRACT

In this study, Al/(ZnO-PVA)/p-Si (MPS) type Schottky diodes (SDs) were produced and the radiation effects on their electrical properties were investigated using the current-voltage ( $I-V$ ) measurements. The  $I-V$  measurements were performed before irradiation and after various irradiation doses in the wide voltage range ( $\pm 4$  V) at room temperature. To determine gamma-irradiation effects on the MPS-type SDs accurately, one SD was preferred as a sample, and its significant electrical parameters such as zero-bias barrier height ( $\phi_{B0}$ ), ideality factor ( $n$ ), and reverse-saturation-current ( $I_0$ ) were calculated using the linear parts of the  $\ln(I)-V$  characteristics. Besides, to observe the effects of gamma-rays on MPS-type SDs in different voltage regions, some diode parameters were obtained by different calculation methods such as Cheung and Norde functions as well as Thermionic Emission (TE) theory. The calculations showed that high doses of gamma-irradiation ( $>5$  kGy) caused the annealing effect, which leads to an improvement in some electrical parameters of SD, especially in the high electric field region. On the other hand, the energy distribution of the surface states ( $N_{ss}$ ) was obtained by utilizing the voltage-dependent ideality factor and the effective barrier height, with and without considering the series resistance ( $R_s$ ) effect. It was observed that  $N_{ss}$  values decreased almost exponentially from the mid-band gap of the semiconductor towards the upper edge of the valence-band. Also, the density of surface states decreased with increasing radiation doses. As a result, almost all diode parameters are affected by irradiation. However, no significant defect has been detected that would affect the stable operation of the diode. Hence, Al/(ZnO-PVA)/p-Si type SD can be used as an MPS-type detector instead of MIS/MOS-type detectors due to some advantages of the organic/polymer interlayer such as being cheap, light per molecule, flexible and requiring low energy consumption.

### 1. Introduction

Over the past two decades, researchers have focused on fabricating organic/polymer interlayered metal-semiconductor (MS) structures to control the carrier mechanisms and barrier height. Organic interlayers are cheaper, lighter per molecule, and flexible than the conventional insulator/oxide interlayers. They have also inexpensive growth methods such as electrospinning and sol-gel (Altindal-Yerişkin et al., 2017; Demirezen and Altindal Yerişkin, 2020; Ersöz et al., 2016). Organic or insulator interlayers used in MS structures provide metal and

semiconductor layers isolation and contribute to the regulation of charge transmissions. Metal-insulator/polymer-semiconductor (MIS/MPS) type structures have series resistance ( $R_s$ ) and surface states ( $N_{ss}$ ) and any voltage applied to the material is distributed over the series resistance, depletion layer, and the interfacial layer. Therefore, the electrical properties of these structures deviate from their ideal behaviour under such conditions as illumination or radiation. In other words, both the electrical and optical properties of MIS/MPS-type structures considerably depend on the  $R_s$ ,  $N_{ss}$  and applied electric field as well as radiation, interfacial layer, and the doping of the

\* Corresponding author.

E-mail address: [ahmetkaymaz@karabuk.edu.tr](mailto:ahmetkaymaz@karabuk.edu.tr) (A. Kaymaz).

semiconductor (Akhlaghi et al., 2018; Alptekin and Altundal, 2019; Boughdachi et al., 2018; Buyukbas-Ulusan et al., 2018; Khanna et al., 2005; Reddy, 2014; Rhoderick and Williams, 1988; Sekhar Reddy et al., 2016; Sze and Ng, 2006). On the other hand, surface states located between the interfacial layer and semiconductor react as recombination centres and they can be able to capture or release some electrical charges under electric field or radiation. These centres also provide a tunnelling pathway for the carriers (Arslan et al., 2009; Card and Rhoderick, 1971).

In this study, due to its considerable superior features, ZnO doped-PVA was preferred as an organic interlayer instead of traditional insulator/oxide interlayer. For example, PVA has a high-capacity of charge storage and high strength as well as it is a semi-crystalline, nontoxic, and water-soluble material (Altindal-Yerişkin et al., 2017; Demirezen and Altindal Yerişkin, 2020; Ersöz et al., 2016). Furthermore, its conductivity and dielectric permittivity can be controlled by doping a suitable metal or metal-oxide material. Then again, ZnO is a direct band-gap semiconductor and due to its high transparency in the visible range, it can be preferred as a window material. ZnO can be also used as a potential transparent conducting oxides material in optoelectronics (Vijayalakshmi et al., 2008). Besides, the large exciton binding energy (60 meV) of ZnO provides thermal stability in solar cells.

Semiconductor-based materials such as SDs, solar cells, MOS capacitors, and transistors are widely used in electronic devices which are efficaciously taking part in satellite systems and medical applications. However, these materials are quite sensitive to some types of ionizing radiation and can be adversely affected by magnetic fields, electric fields, charged particles, solar radiation, galactic radiation, etc. (Binder et al., 1975; Laha et al., 2012). Also, biomedical materials are intensively used under radiation influences. Although the importance of these materials in such electronic systems cannot be ignored, the electrical and optical characteristics of these structures can be easily affected by electromagnetic radiations such as  $\alpha$ ,  $\beta$ ,  $\gamma$  and  $\gamma$  rays (Ali et al., 2013). Therefore, the radiation-induced defects may cause to degrade the device performance (Altindal et al., 2005; Tian and Cao, 2016).

Among the generated electron-hole pairs under radiation, having less mobility than electrons, holes can easily diffuse to the interfacial layer. On the other hand, the electrons either recombine with the holes or move out of the interfacial layer (Dökme et al., 2008; Dökme and Altindal, 2012; Feteah et al., 2002; Maurya and Awasthi, 2018; Tataroğlu et al., 2007; Tüzün et al., 2008; Uslu et al., 2012; Winokur et al.). Since the radiations rarely do not contain enough energy to form electron-hole pairs, many energetic particles and photons cannot be absorbed by a semiconductor and that causes their direct passing through devices.

Many researchers have studied the effects of ionizing radiation on semiconductor-based materials (Ali et al., 2013; Khanna et al., 2005; Laha et al., 2012; Matoussi et al., 2005; Paradvah et al., 2016; Sahin and Kabacılık, 2018; Srour and Palko, 2013; Teffahi et al., 2016; Tobnaghi et al., 2014; Uslu et al., 2012; Vijayalakshmi et al., 2008). However, when voltage and radiation are evaluated together, these effects have not been fully explained yet. Moreover, if a different type of material is preferred as the interfacial layer or if the type and/or the dose of the radiation change, the impact of the radiation on the material would change considerably. Then again, it is generally expected that both radiation and temperature affect the performance of SDs negatively, but this estimation is not always correct. This is why the investigation of the radiation effects on SDs or other semiconductor-based structures and the determination of the degree of hardness of these devices against radiation are significant issues to be handled. Besides, production of the radiation-resistant structures is quite important to enhance the operational reliability of the electronic components which have possible use in industrial application, biomedical devices, and satellite systems. Therefore, this study aims to produce ZnO doped-PVA interfacial-layered MPS-type SDs instead of traditional MIS/MPS-type structures. Besides, it is aimed to understand the effects of voltage and gamma-irradiation on MPS-type structures, accurately and

comprehensively. To achieve these objectives, the main electrical parameters such as  $I_0$ ,  $n$ ,  $\Phi_{BO}$ ,  $R_s$ , and shunt resistance ( $R_{sh}$ ) were calculated before and after various radiation doses utilizing the  $I-V$  characteristics of SD. As a result, it has been observed that almost all diode parameters vary depending on radiation and voltage. However, no significant defect or deterioration has been detected which would affect the stable operation of Al/(ZnO-PVA)/p-Si type SD.

## 2. Experimental details

The production of Al/(ZnO-PVA)/p-Si type SDs was completed performing the following main steps. Besides, more detailed information about the fabrication process is available in reference (Kaymaz et al., 2020), while the preparation process of the organic solution (ZnO-PVA) is available in reference (Nezhadesm-Kohardafchahi et al., 2018).

- a) 300  $\mu\text{m}$  thick p-Si type semiconductor wafers were chemically cleaned to remove the natural oxide layers and other organic impurities on them.
- b) The metal (99.999% pure Al) was thermally evaporated onto the whole backside of the p-Si wafers at  $10^{-6}$  Torr with 120 nm thicknesses and then to get low-resistivity ohmic contact, Al/p-Si type wafers were annealed at 450 °C in  $\text{N}_2$  ambient.
- c) The prepared ZnO-PVA solution was grown on the front surface of the p-Si wafers using the spin coating technique. It is known that the thickness of the interfacial layer can be calculated using the capacitance-conductance-voltage ( $C-G/\omega-V$ ) characteristics, for which relevant characteristics are available in reference (Kaymaz et al., 2020) for Al/(ZnO-PVA)/p-Si type SD. According to Nicollian and Brews (2003), the value of the interfacial layer capacitance ( $C_i$ ) can be obtained using Eq. (1) from the capacitance ( $C_{ma}$ ) and conductance ( $G_{ma}/\omega$ ) values in the strong accumulation region, whose measurements are carried out at high frequency ( $f \geq 500$  kHz). It is also known that there is a relationship between the capacitance and thickness of the interfacial layer as in Eq. (2) (Nezhadesm-Kohardafchahi et al., 2018; Orak et al., 2017; Taççıoğlu et al., 2017). In these equations,  $\epsilon'$  (=8.5) is the permittivity of the interlayer (Nezhadesm-Kohardafchahi et al., 2018),  $\epsilon_0$  (=8.85  $\times 10^{-14}$  F/cm) is the permittivity of vacuum,  $A$  (=7.85  $\times 10^{-3}$  cm $^2$ ) is the rectifier contact area and  $d_i$  is the thickness of the interfacial later. Thus, the thickness of the ZnO-PVA organic interlayer can be calculated using the relevant equations, and the thickness of the interfacial layer was obtained as 81 Å.

$$C_i = C_{ma} \left[ 1 + \left( \frac{G_{ma}}{\omega C_{ma}} \right)^2 \right] \quad (1)$$

$$d_i = \frac{\epsilon' \epsilon_0 A}{C_i} \quad (2)$$

- d) Finally, high-purity Al was evaporated thermally onto the surface of the organic (ZnO-PVA) interlayer and so, it was obtained dots with 7.85  $\times 10^{-3}$  cm $^2$  area and 120 nm thick. Consequently, the production process of Al/(ZnO-PVA)/p-Si type SDs was completed and the schematic cross-section of the MPS-type SD is given in Fig. 1.

The forward and reverse bias  $I-V$  measurements were performed before irradiation and after various irradiation doses (1, 5, 10, 30 and 60 kGy) via the Keithley 2400  $I-V$  Source Meter and IEEE-488 AC/DC converter card. To eliminate the external effects and noises, the measurements were carried out in the VPF-475 cryostat at  $10^{-3}$  Torr pressure. The detailed scheme of the measurement system is given in Fig. 2. On the other hand, the irradiation process of the sample was carried out using the Ob-Servo Sangius Co-60 irradiation source at the Saraykoy Nuclear Research and Training Center of Turkish Atomic Energy Authority at a dose rate of 1296 Gy/h and a total dose of 60 kGy.

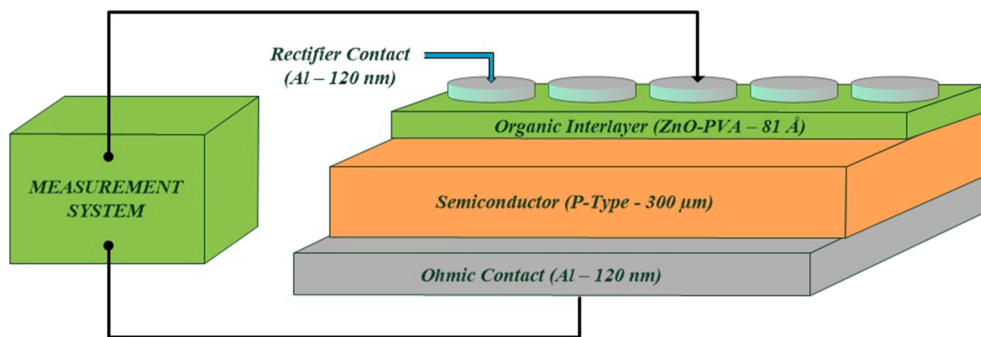


**Fig. 1.** The schematic cross-section of Al/(ZnO-PVA)/p-Si (MPS) type SD.

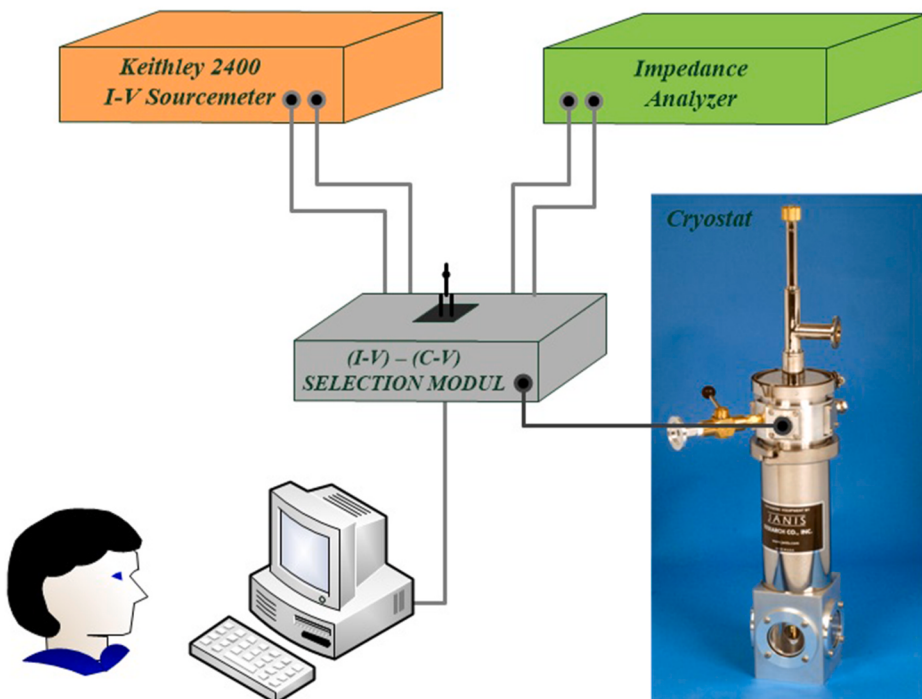


**Fig. 2.** The detailed scheme of the measurement system.

### 3. Results and discussion

In general, radiation is expected to have two effects as temporary and permanent on materials (Güllü et al., 2008a). The permanent effect, resulting in the change of crystal lattice structure, is mostly caused by radiation bombardment. The radiation-induced generation or recombination of electron-hole pairs occur as a temporary effect on materials. However, eight effects may occur in irradiated devices, in which one or more effects can be effective simultaneously (Srour et al., 2003). As a result, the performance of irradiated devices is highly affected by radiation-induced defects, interface traps, dangling bonds, recrystallization, etc. (Badila et al., 2001; García et al., 2009). To understand these effects accurately and comprehensively, the detailed analysis of the measurements should be performed. Therefore, in this study, radiation effects on Al/(ZnO-PVA)/p-Si type SDs were investigated using  $I$ - $V$  characteristics. The  $I$ - $V$  characteristics of Al/(ZnO-PVA)/p-Si type SD before irradiation and after various irradiation doses (1, 5, 10, 30, and 60 kGy) are given in Fig. 3. The linear parts of the forward bias  $\ln(I)$ - $V$  characteristics are also shown in this figure due to their use in the calculations. Currents have been logarithmically plotted to be able to evaluate the reverse and forward biases currents together. As can be seen in Fig. 3 and Table 1, there is an increment in the reverse bias

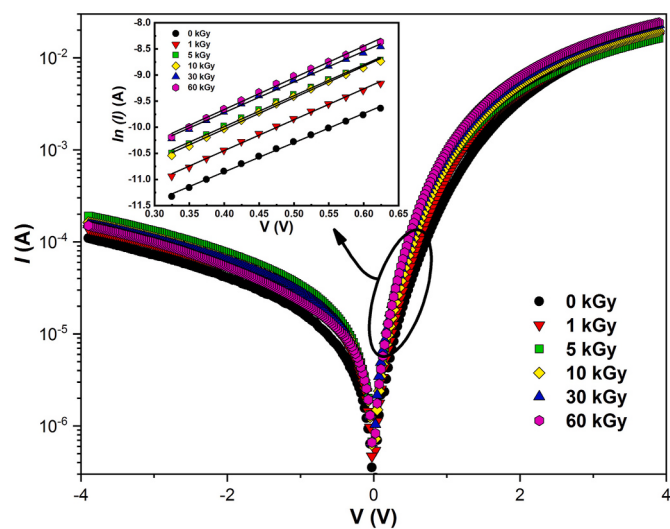


**Fig. 3.** The  $I$ - $V$  characteristics of MPS-type SD before and after gamma-irradiation.

**Table 1**

The main electrical parameters of MPS-type SD before and after irradiation.

Irradiation Doses (kGy)	The Main Diode Parameters						
	$I_F$ (A) (at +4 V)	$I_R$ (A) (at -4 V)	$I_0$ (A)	n	$\Phi_{BO}$ (eV)	$R_s$ (Ω)	$R_{sh}$ (kΩ)
0	$1.96 \times 10^{-02}$	$1.14 \times 10^{-04}$	2.05 × $10^{-6}$	6.901	0.601	204	35.2
1	$1.80 \times 10^{-02}$	$1.44 \times 10^{-04}$	2.76 × $10^{-6}$	6.539	0.593	222	27.7
5	$1.70 \times 10^{-02}$	$1.98 \times 10^{-04}$	4.12 × $10^{-6}$	6.528	0.583	236	20.3
10	$2.04 \times 10^{-02}$	$1.69 \times 10^{-04}$	4.12 × $10^{-6}$	6.420	0.583	196	23.7
30	$2.40 \times 10^{-02}$	$1.59 \times 10^{-04}$	5.56 × $10^{-6}$	6.584	0.575	167	25.2
60	$2.52 \times 10^{-02}$	$1.57 \times 10^{-04}$	5.56 × $10^{-6}$	6.377	0.575	158	25.5

currents up to 5 kGy radiation doses and then these currents tend to decrease up to 60 kGy doses. Whereas forward bias currents decrease up to 5 kGy doses and then they show an increasing trend with larger doses as the opposite behaviour of the reverse bias currents. The increase in currents because of the radiation is attributed to the presence of the new charge carriers and the great number of defects near the semiconductor because such defects provide pathways to the charge carriers (Barala et al., 2015). Another reason for the increment in currents may be the decrease in barrier height or the reduction of recombination centres near the semiconductor (Teffahi et al., 2016). But then, the increase in the forward bias currents and the decrease in the reverse bias currents, at doses above 5 kGy, are thought to be due to the annealing effect of high doses of gamma-rays. However, some electrical parameters of SD such as  $I_0$ , n, and  $\Phi_{BO}$  should also be calculated to acquire more information about the gamma-irradiation effects. The calculation methods of the mentioned parameters are discussed below.

It is known that the Thermionic Emission (TE) Theory can be used to obtain some electrical parameters of SDs (Sze and Ng, 2006). According to TE, there is a relationship between the current and voltage of the diode in the positive intermediate voltage region as in Eq. (3). In this equation,  $I_0$  corresponds to the reverse-saturation-current and its formula is given by Eq. (4). Also, other symbols are well known in the literature (Sze and Ng, 2006). In other respect, if Eq. (3) is organized, Eq. (5) can be obtained and using this equation the formula for n can be written as in Eq. (6). Thus,  $I_0$  and n can be extracted from the linear parts of the  $\ln(I)$ -V characteristic such as  $y=mx+a$ . Since  $I_0$  is calculated from Eq. (5)  $\Phi_{BO}$  can also be obtained using Eq. (7) which is extracted from Eq. (4). As a result,  $I_0$  values are obtained from the intersection of the linear parts of the forward bias  $\ln(I)$ -V characteristics with the current's axis, while n and  $\Phi_{BO}$  are obtained using the slope of the linear parts of the same plots. Besides,  $R_{sh}$  and  $R_s$  can be calculated using the sufficient reverse and forward bias I-V characteristics by Ohm's laws. Thus, the main diode parameters, which are extracted by these equations, are demonstrated in Table 1. As can be seen in Tables 1 and  $I_0$  values increase with increasing irradiation doses. An increase or a decrease in  $I_0$  values is attributed to the fact that deep levels act as generation or recombination centres (Mamor et al., 2007). Any decrement in barrier height can also lead up to an increment in these currents (Teffahi et al., 2016).

$$I = I_0 \left[ \exp\left(\frac{qV}{nkT}\right) - 1 \right] \quad (3)$$

$$I_0 = AA^* T^2 \exp\left(-\frac{q\Phi_{BO}}{kT}\right) \quad (4)$$

$$\ln(I) = \ln \left[ I_0 \left( \exp\left(\frac{qV}{nkT}\right) - 1 \right) \right] = \ln(I_0) + \left( \frac{q}{nkT} \right) \cdot V = m \cdot x + a \quad (5)$$

$$n = \frac{q}{kT} \left( \frac{dV}{d(\ln(I))} \right) = \frac{q}{mkT} \quad (6)$$

$$\Phi_{BO} = \frac{kT}{q} \ln \left( \frac{AA^* T^2}{I_0} \right) \quad (7)$$

The n values obtained before irradiation and after various irradiation doses are considerably greater than unity. This is attributed to the existence of other possible carrier mechanisms (diffusion theory, generation-recombination theory, tunnelling caused by surface states and dislocation, Gaussian distribution of the barrier height) together with TE theory. According to Gaussian distribution theory, carriers, which do not have enough energy to cross the barrier, can through a large number of obstacles or pathways present in the vicinity of the average obstacle. This leads to an increase in currents and n values. The high n values obtained before and after irradiation are evidence of the deviation from the standard TE theory. In other respect, it was observed that the n values tended to decrease almost regularly with increasing irradiation doses. The decrease in n values with increasing irradiation doses can be evaluated as an interesting behaviour. However, this behaviour can occur with the expansion of the depletion layer width ( $W_D$ ) and the decrease of the density of surface states according to Eq. (16) which is given by Card and Rhoderick. This equation shows that the ideality factor is directly proportional to the density of the surface states and inversely proportional to the depletion layer width. The variation of the depletion layer width depending on radiation, which is given in reference (Kaymaz et al., 2020), and Fig. 11, where the density of the surface states are shown, also support this information. Again, in another study, it is noticed that interfacial trap centres are annealed in consequence of secondary electrons generated by gamma-irradiation and this results in reduction (improvement) of n values (Verma et al., 2014).

Experimental results have shown that  $\Phi_{BO}$  values decrease with increasing irradiation doses. According to some researchers, gamma-irradiation induces defects in the band-gap at the junction of the semiconductor and this affects the free carrier concentration (Fonash et al., 1981; Grusell et al., 1980). The change in the carrier concentration means a decrease or an increase in the barrier height of the structures. Yannan Xu et al. determined the degradation on the electrical characteristics of SDs including the decrease of the barrier height after exposure the devices to the gamma-ray source (Xu et al., 2019). X-ray photoelectron spectroscopy analysis, a part of their study (Xu et al., 2019), confirmed defects creation in Si dangling bonds. These defects caused a reduction in barrier height and enhanced tunnelling effects, which result in a significant increase in the currents. It is known that the annealing effect of gamma-rays can cause a reduction in the barrier height and/or improvement in the electrical parameters of devices (Bobby et al., 2014; Kumar et al., 2017; Srour et al., 2003; Vijayalakshmi et al., 2008).

The annealing effect may occur on the materials as a result of the high electronic energy loss of gamma-rays (Kumar et al., 2017). The annealing effect is one of the radiation-induced defects and it causes an increment in the effectiveness of the thermal creation of the carriers (Srour et al., 2003). When the materials are exposed to high radiation doses, some defects may occur on them and if these defects are in a region of the high electric field, the annealing effect is expected to occur on these materials. At the high radiation doses (>5 kGy), the improvement in  $R_s$  and  $R_{sh}$  values obtained from the high voltage/electric-field regions is evidence that the annealing effect occurs in this SD.

Resistance values are crucial parameters for the structure to specify

defect or noise rate caused by radiation. The real  $R_s$  and  $R_{sh}$  values of SDs can be calculated using the sufficiently forward and reverse bias current and voltage values (4 V and -4 V). The voltage-dependent resistance ( $R_i$ -V) plots of the diode before and after irradiation are shown in Fig. 4. As can be seen in Fig. 4 and Table 1, the greater change occurs in  $R_{sh}$  values compared to  $R_s$  values after irradiation. This is because of the more changing of the reverse bias currents than the forward bias currents. It was also observed that  $R_i$  values were affected a lot due to the radiation-induced defects. It is known that trap levels can reduce or increase the free carrier density of the structures, which may lead to an increase or a decrease in the diode's resistance (Tian and Cao, 2016). On the other hand, when the real resistance values before irradiation and after the highest dose of irradiation (60 kGy) are compared, it is seen that  $R_s$  and  $R_{sh}$  values decrease after radiation. This decrement may be ascribed by the radiation induced-defects in the energy gap at the junction of the interface (Güllü et al., 2008b). Because the increase of electrons in the traps and conduction band leads to an increase in conductivity ( $\sigma$ ) or conductance ( $G$ ) values, and so a decrease in resistance values is observed ( $R = 1/G$ ). Again, when all radiation doses are considered, it can be seen that  $R_s$  values increase up to 5 kGy irradiation doses, and then they tend to decrease with increasing irradiation doses. Whereas, the changes in  $R_{sh}$  values are the opposite of this behaviour. As a result, it can be said that above 5 kGy irradiation doses, there is an improvement in the diode parameters especially obtained from the high electric-field/voltage regions due to the annealing effect of the gamma-rays. This result is obvious evidence that the annealing effect occurs in Al/(ZnO-PVA)/p-Si type SD. Now let us examine other calculation methods to support this result.

Significant electrical parameters of SDs such as  $n$ ,  $\Phi_B$ , and  $R_s$  can be calculated using Cheung-I and Cheung-II functions (Cheung and Cheung, 1986) as well as the TE. Eq. (8), which corresponds to the forward bias current expression in which series resistance is also considered, can be used to obtain Eqs. (9) and (10). According to Cheung functions, if  $dV/d(\ln(I))$  are plotted to versus  $I$ ,  $R_s$  and  $n$  can be extracted from the slope and intersection of the linear part of this plot. Similarly,  $R_s$  and  $\Phi_B$  can be calculated using the linear part of the  $H(I)$ -I plot. Norde function can also be used as another method (Norde, 1979) to calculate some diode parameters such as  $R_s$  and  $\Phi_B$ . Norde's modified method is given by Eq. (11) where  $\gamma$  corresponds to an integer greater than  $n$  which is extracted from the  $\ln(I)$ -V plot. Again,  $\Phi_B$  can be obtained as in Eq. (12) using the  $F(V_0)$ , which is the minimum value of  $F(V)$ . Then, the  $R_s$  value is obtained using Eq. (13). The plots of the linear regions of  $dV/d(\ln(I))$ -I and  $H(I)$ -I before and after irradiation are given in Fig. 5 and

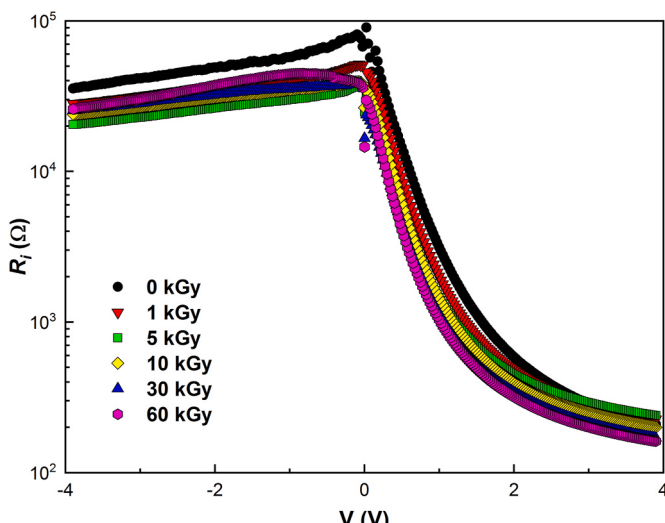


Fig. 4. The  $R_i$ -V characteristics of MPS-type SD before and after gamma-irradiation.

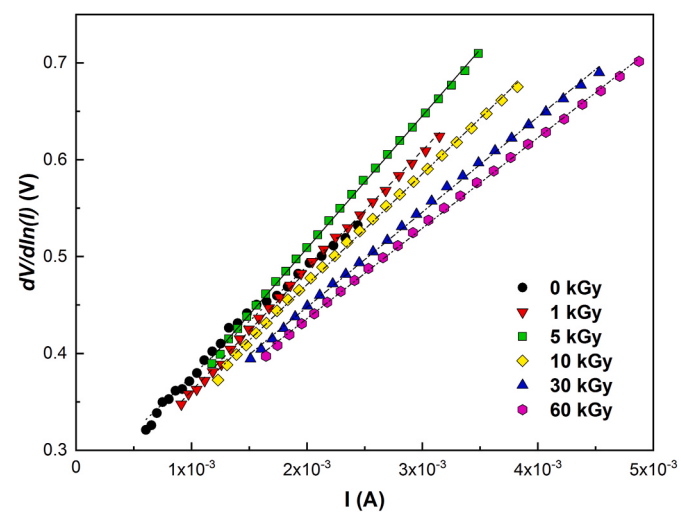


Fig. 5. The linear regions of  $dV/d(\ln(I))$ -I plots for before and after gamma-irradiation.

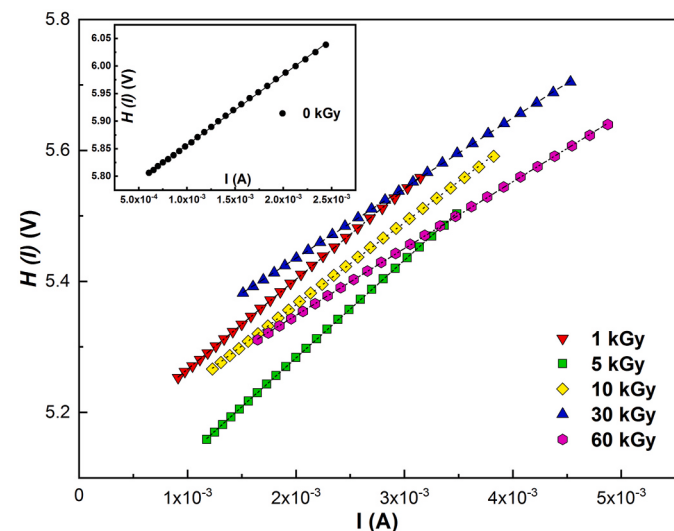


Fig. 6. The linear regions of  $H(I)$ -I plots for before and after gamma-irradiation.

Fig. 6, respectively. while the  $F(V)$ -V plots are given in Fig. 7. The main diode parameters, which were obtained from the Cheung and Norde functions as well as TE theory, are demonstrated in Table 2. Also, the variations of the  $n$  and  $\Phi_B$  depending on voltage and gamma-irradiation are demonstrated in Fig. 8. This figure clearly shows the effects of radiation in different voltage regions. For example, the crossing of the  $\Phi_B$  curves at a voltage value of around 2.75 V reveals the annealing effect of gamma-irradiation in the high electric-field/voltage region.

$$I = I_0 \exp\left(\frac{qV(I - R_s)}{nkT}\right) \quad (8)$$

$$\frac{dV}{d(\ln I)} = \frac{nkT}{q} + IR_s \quad (9)$$

$$H(I) = V - \frac{nkT}{q} \ln\left(\frac{I}{AA^*T^2}\right) = n\Phi_B + IR_s \quad (10)$$

$$F(V) = \frac{V}{\gamma} - \frac{kT}{q} \ln\left(\frac{I(V)}{AA^*T^2}\right) \quad (11)$$

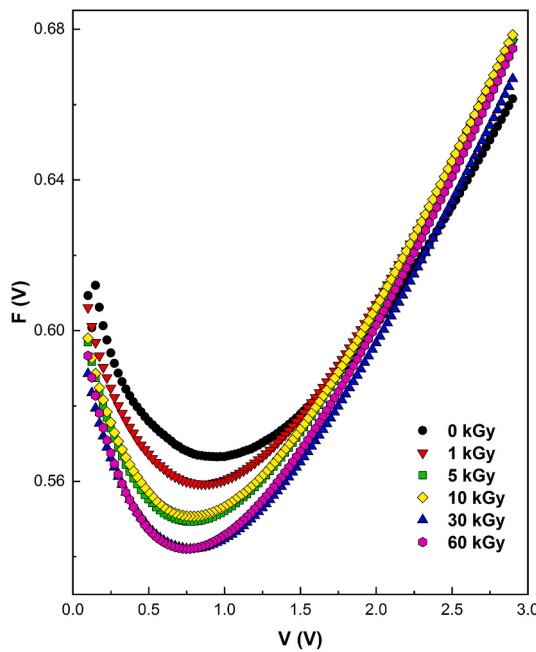


Fig. 7. The  $F(V)$ - $V$  plots of MPS-type SD before and after irradiation.

$$\Phi_B = F(V_0) + \frac{V_0}{\gamma} - \frac{kT}{q} \quad (12)$$

$$R_s = \frac{kT(\gamma - n)}{qI} \quad (13)$$

The results obtained by different calculation methods seem to be inconsistent with each other. However, considering the natural calculation methods and the voltage dependence of these parameters, it can be inferred that the values of these parameters are quite compatible with each other. For example, the parameters calculated using Cheung's functions were obtained from the voltage range of 1.2 V–1.8 V while the parameters calculated using  $\ln(I)$ - $V$  plots were obtained from the voltage range of 0.325 V–0.625 V. Cheung functions take into account the current values measured from the point where the graphs of the forward bias current begin to bend, whereas, Norde functions consider all forward bias current values in their calculations (Güllü et al., 2008a). Therefore, as can also be seen in Table 2,  $R_s$  values acquired from Norde's method were found higher than  $R_s$  values acquired from Cheung's methods. The plots of the real  $R_s$  values, which are changed depending on radiation and calculation methods, are shown in Fig. 9 to be able to observe the differences between the calculation methods (TE, Cheung and Norde) more clearly. Plots showing the changes in the  $\Phi_B$  values depending on calculation method and radiation are also given in Fig. 10.

The voltage-dependent ideality factor ( $n(V)$ ) and the effective barrier height ( $\Phi_e$ ) should be obtained to calculate radiation-induced surface states in the band-gap. The  $n(V)$  and  $\Phi_e$  can be calculated using Eqs. (14)

and (15) when the  $R_s$  effect is neglected (Tataroğlu and Altindal, 2007). Thus, the  $N_{ss}$  formula can be written as in Eq. (16) by taking into account  $n(V)$  and  $\Phi_e$  (Card and Rhoderick, 1971). If  $R_s$  effect is considered,  $(V - IR_s)$  expression should be used instead of  $(V)$  expression in these formulas. In these equations,  $\epsilon_s$  and  $\epsilon_i$  correspond to the permittivity of the semiconductor and the permittivity of the interlayer, respectively.  $\delta$  is the thickness of the polymer interlayer (ZnO-PVA) and its value was obtained as 81 Å for this diode (Kaymaz et al., 2020). On the other hand, it is known that the energy formula from the mid-gap ( $E_{ss}$ ) towards the upper edge of the valence band ( $E_v$ ) is given by Eq. (17) for p-type

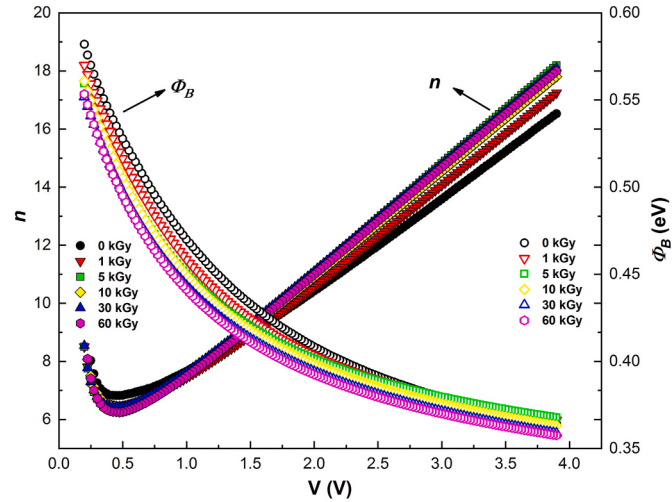


Fig. 8. The ideality factor and the barrier height depending on voltage and radiation.

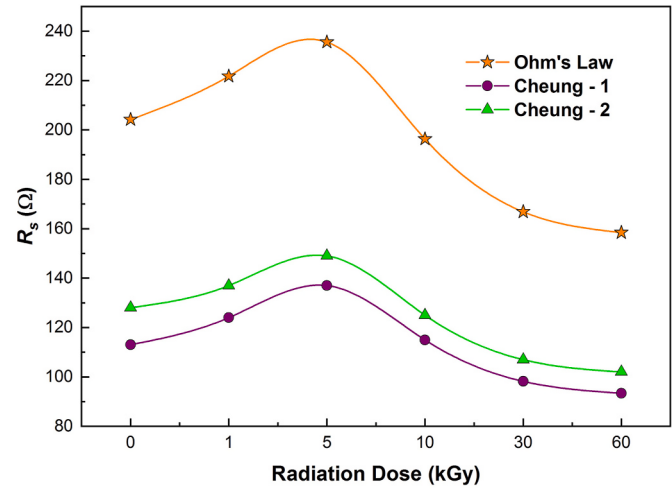


Fig. 9. The variation of real  $R_s$  values depending on radiation and calculation methods.

Table 2

Some electrical parameters of SD obtained by different calculation methods.

Irradiation Doses (kGy)	$I$ - $V$			Cheung-I		Cheung-II		Norde	
	n	$\Phi_{B0}$ (eV)	$R_s$ ( $\Omega$ )	n	$R_s$ ( $\Omega$ )	$\Phi_B$ (eV)	$R_s$ ( $\Omega$ )	$\Phi_B$ (eV)	$R_s$ ( $\Omega$ )
0	6.901	0.601	204	10.164	113	0.564	128	0.618	608
1	6.539	0.593	222	9.159	124	0.560	137	0.615	363
5	6.528	0.583	236	9.082	137	0.548	149	0.605	244
10	6.420	0.583	196	9.353	115	0.546	125	0.608	240
30	6.584	0.575	167	9.739	98.2	0.536	107	0.597	191
60	6.377	0.575	158	9.623	93.4	0.534	102	0.600	168

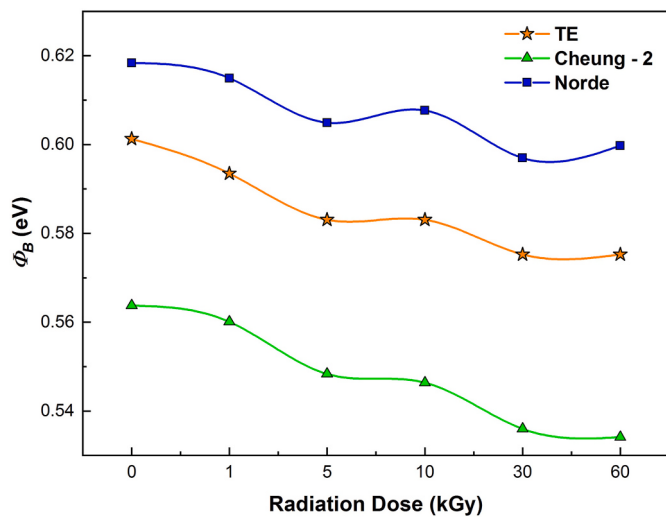


Fig. 10. The variation of barrier height depending on radiation and calculation methods.

semiconductor. Thus, the energy-dependent  $N_{ss}$  profiles can be acquired by using these equations.

$$n(V) = \frac{q}{kT} \left( \frac{V}{\ln(I/I_0)} \right) \quad (14)$$

$$\Phi_e = \Phi_{B0} + \left( 1 - \frac{1}{n(V)} \right) (V) \quad (15)$$

$$N_{ss} = \frac{1}{q} \left[ \frac{\epsilon_i}{\delta} (n(V) - 1) - \frac{\epsilon_s}{W_D} \right] \quad (16)$$

$$E_{ss} - E_v = q(\Phi_e - V) \quad (17)$$

The energy-dependent  $N_{ss}$  profiles before irradiation and after various irradiation doses are given in Fig. 11. As can be seen in this figure, the density of surface states decreases almost as exponentially from the  $E_{ss}$  towards the upper edge of the  $E_v$  for before and after irradiation. Also, the  $N_{ss}$  values decrease almost regularly with increasing radiation doses. This behaviour of  $N_{ss}$  is attributed to the recombination of electron-hole pairs under radiation and/or reordering/restructuring of the band-gap surface states under electric field (Kaya et al., 2014). On the other hand, it can be observed that the  $N_{ss}$  values are quite low while taking into account the  $R_s$  effect. This result clearly reveals the importance of  $R_s$  in the calculations.

#### 4. Conclusion

Gamma-irradiation effects on the electrical parameters of Al/(ZnO-PVA)/p-Si (MPS) type SDs have been investigated using the  $I-V$  measurements which were carried out in the wide range of voltage ( $\pm 4V$ ) and radiation dose (0–60 kGy). The main electrical parameters such as  $I_0$ ,  $n$ ,  $\Phi_B$ ,  $R_s$  and  $R_{sh}$  were obtained before and after irradiation to determine the effects of radiation accurately on this SD. Also, some diode parameters such as  $n$ ,  $R_s$  and  $\Phi_B$  were obtained by using Cheung and Norde methods, which consider different voltage regions in their calculations, to understand the effects of radiation in different voltage regions. The energy-dependent profiles of the surface states were also obtained with and without  $R_s$  effect considering  $n(V)$  and  $\Phi_e$ . Thus, the following important results were observed: a)  $I_0$  values increased with increasing irradiation doses. This increment was attributed to deep levels acting as generation centres and the reduction in barrier height. b) There was a decrease in  $n$  values due to the gamma-irradiation effects. This behaviour was attributed to the expansion of the depletion layer width and the decrease in  $N_{ss}$  values under radiation. c) The barrier

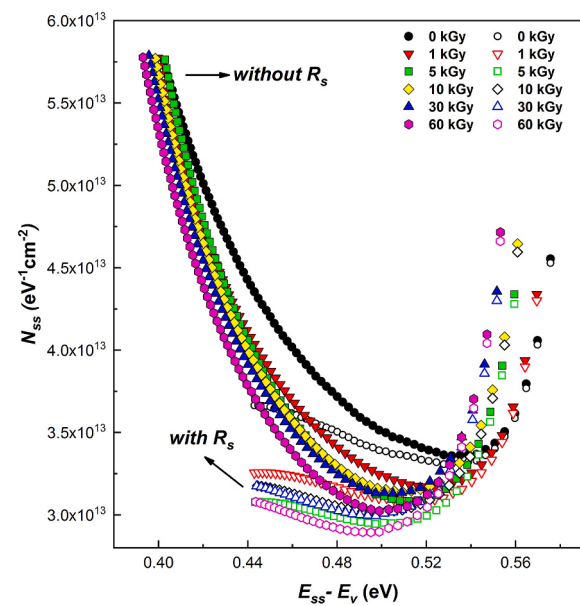


Fig. 11. The energy distribution of the surface states depending on gamma-irradiation.

height decreased with increasing irradiation doses. This decrement was attributed to the radiation-induced defects, the defect creation in Si dangling bonds and the annealing effect of gamma-rays. d) The  $R_s$  values increased up to 5 kGy irradiation doses and they showed a decreasing trend at higher doses. Whereas the changes in  $R_{sh}$  depending on radiation were the opposite of this behaviour. The decrease in  $R_s$  values in high doses of gamma-irradiation (> 5 kGy), especially in the high electric field region, revealed the annealing effect of gamma-rays.

As a result, all diode parameters were affected by gamma-irradiation. However, no significant defect was observed that implicitly affect the stable operation of Al/(ZnO-PVA)/p-Si type SD. Therefore, this SD can be used as MPS-type detector instead of MIS/MOS type detectors due to some of the organic/polymer interlayer advantages such as being cheap, light per molecule, flexible and requiring low energy consumption. This result is a crucial determination for the safe operation of satellite systems, biomedical devices and other electronic components operating under the influence of radiation.

#### CRediT authorship contribution statement

**Ahmet Kaymaz:** Conceptualization, Methodology, Validation, Formal analysis, Investigation, Measurements, Writing – original draft, and Visualization. **Esra Evcin Baydilli:** Methodology, Validation, Investigation, Measurements, Writing – original draft, and Visualization. **Habibe Uslu Tecimer:** Conceptualization, Methodology, Validation, Formal analysis, Resources, Writing – review & editing. **Semsettin Altindal:** Validation, Resources, Supervision, Project administration, Funding acquisition. **Yashar Azizian-Kalandaragh:** Preparation of the samples.

#### Declaration of competing interest

The authors declare that they have no known competing financial interests or personal relationships that could have appeared to influence the work reported in this paper.

#### Acknowledgements

This study was supported by Projects of Scientific Investigation (BAP), Gazi University, Ankara, Turkey. Project Number: GU-BAP.05/

2019–26.

## References

- Akhlaghi, E.A., Badali, Y., Altindal, S., Azizian-Kalandaragh, Y., 2018. Preparation of mixed copper/PVA nanocomposites as an interface layer for fabrication of Al/Cu-PVA/p-Si Schottky structures. *Phys. B Condens. Matter* 546, 93–98. <https://doi.org/10.1016/j.physb.2018.06.019>.
- Ali, K., Khan, S.A., MatJafri, M.Z., 2013. 60Co  $\gamma$ -irradiation effects on electrical characteristics of monocrystalline silicon solar cell. *Int. J. Electrochem. Sci.* 8, 7831–7841.
- Alptekin, S., Altindal, S., 2019. A comparative study on current/capacitance: voltage characteristics of Au/n-Si (MS) structures with and without PVP interlayer. *J. Mater. Sci. Mater. Electron.* 30, 6491–6499. <https://doi.org/10.1007/s10854-019-00954-5>.
- Altindal-Yerişkin, S., Balbaşı, M., Orak, İ., 2017. The effects of (graphene doped-PVA) interlayer on the determinative electrical parameters of the Au/n-Si (MS) structures at room temperature. *J. Mater. Sci. Mater. Electron.* 28, 14040–14048. <https://doi.org/10.1007/s10854-017-7255-1>.
- Altindal, S., Tataroğlu, A., Dökme, İ., 2005. Density of interface states, excess capacitance and series resistance in the metal-insulator-semiconductor (MIS) solar cells. *Sol. Energy Mater. Sol. Cells* 85, 345–358. <https://doi.org/10.1016/j.solmat.2004.05.004>.
- Arslan, E., Altindal, S., Özçelik, S., Ozbay, E., 2009. Tunneling current via dislocations in Schottky diodes on AlInN/AlN/GaN heterostructures. *Semicond. Sci. Technol.* 24 <https://doi.org/10.1088/0268-1242/24/7/075003>, 075003.
- Badila, M., Godignon, P., Millan, J., Berberich, S., Brezeanu, G., 2001. The electron irradiation effects on silicon gate dioxide used for power MOS devices. *Microelectron. Reliab.* 41, 1015–1018. [https://doi.org/10.1016/S0026-2714\(01\)00060-9](https://doi.org/10.1016/S0026-2714(01)00060-9).
- Barala, S.S., Singh, J., Ranwa, S., Kumar, M., 2015. Radiation induced response of Ba-0.5Sr-0.5TiO<sub>3</sub> based tunable capacitors under gamma irradiation. *IEEE Trans. Nucl. Sci.* 62, 1873–1878. <https://doi.org/10.1109/TNS.2015.2449991>.
- Binder, D., Smith, E.C., Holman, A.B., 1975. Satellite anomalies from galactic cosmic rays. *IEEE Trans. Nucl. Sci.* 22, 2675–2680.
- Bobby, A., Shiawakoti, N., Verma, S., Gupta, P.S., Antony, B.K., 2014. Enhancement in electrical properties of Au/n-GaAs Schottky diodes exposed to 60Co gamma rays. *Mater. Sci. Semicond. Process.* 21, 116–121. <https://doi.org/10.1016/j.mssp.2014.01.039>.
- Boughdachi, S., Badali, Y., Azizian-Kalandaragh, Y., Altindal, 2018. Current-transport mechanisms of the Al/(Bi2SS3-PVA nanocomposite)-p-Si Schottky diodes in the temperature range between 220 K and 380 K. *J. Electron. Mater.* 47, 6945–6953. <https://doi.org/10.1007/s11664-018-6593-y>.
- Buyukbas-Ulusun, A., Altindal-Yerişkin, S., Tataroğlu, A., 2018. Forward and reverse bias current-voltage (I-V) characteristics in the metal-ferroelectric-semiconductor (Au/SrTiO<sub>3</sub>/n-Si) structures at room temperature. *J. Mater. Sci. Mater. Electron.* 29, 16740–16746. <https://doi.org/10.1007/s10854-018-9767-8>.
- Card, H.C., Rhoderick, E.H., 1971. Studies of tunnel MOS diodes I. Interface effects in silicon Schottky diodes. *J. Phys. D Appl. Phys.* 4, 1589–1601. <https://doi.org/10.1088/0022-3727/4/10/319>.
- Cheung, S.K., Cheung, N.W., 1986. Extraction of Schottky diode parameters from forward current-voltage characteristics. *Appl. Phys. Lett.* 49, 85–87. <https://doi.org/10.1063/1.97359>.
- Demirezen, S., Altindal Yerişkin, S., 2020. A detailed comparative study on electrical and photo voltaic characteristics of Al/p-Si photodiodes with coumarin-doped PVA interfacial layer: the effect of doping concentration. *Polym. Bull.* 77, 49–71. <https://doi.org/10.1007/s00289-019-02704-3>.
- Dökme, I., Altindal, S., 2012. The effect of gamma irradiation on electrical and dielectric properties of Al-TiW-Pd2Si/n-Si Schottky diode at room temperature. *Curr. Appl. Phys.* 12, 860–864. <https://doi.org/10.1016/j.cap.2011.11.021>.
- Dökme, I., Durmuş, P., Altindal, S., 2008. Effects of  $\gamma$ -ray irradiation on the C-V and G/ $\omega$ -characteristics of Al/SiO<sub>2</sub>/p-Si (MIS) structures. *Nucl. Instruments methods phys. Res. Sect. B beam interact. With mater. Atoms* 266, 791–796. <https://doi.org/10.1016/j.nimb.2008.01.017>.
- Ersöz, G., Yücedağ, I., Azizian-Kalandaragh, Y., Orak, I., Altindal, S., 2016. Investigation of electrical characteristics in Al/Cds-PVA/p-Si (MPS) structures using impedance spectroscopy method. *IEEE Trans. Electron. Dev.* 63, 2948–2955. <https://doi.org/10.1109/TED.2016.2566813>.
- Feteha, M.Y., Soliman, M., Gomaa, N.G., Ashry, M., 2002. Metal-insulator-semiconductor solar cell under gamma irradiation. *Renew. Energy* 26, 113–120. [https://doi.org/10.1016/S0960-1481\(01\)0012-1](https://doi.org/10.1016/S0960-1481(01)0012-1).
- Fonash, S.J., Ashok, S., Singh, R., 1981. Effect of ion-beam sputter damage on Schottky barrier formation in silicon. *Appl. Phys. Lett.* 39, 423–425. <https://doi.org/10.1063/1.92738>.
- García, H., Duerñas, S., Castán, H., Gómez, A., Bailón, L., Barquero, R., Kukli, K., Ritala, M., Leskelä, M., 2009. Irradiation effect on dielectric properties of hafnium and gadolinium oxide gate dielectrics. *J. Vac. Sci. Technol. B Microelectron. Nanom. Struct.* 27, 416. <https://doi.org/10.1116/1.3021040>.
- Grusell, E., Berg, S., Andersson, L.P., 1980. Electrical defects in silicon introduced by sputtering and sputter-etching. *J. Electrochem. Soc.* 127 (1573) <https://doi.org/10.1149/1.2129953>.
- Güllü, Ö., Çankaya, M., Biber, M., Türüt, A., 2008a. Gamma irradiation-induced changes at the electrical characteristics of organic-based Schottky structures. *J. Phys. D Appl. Phys.* 41 (135103) <https://doi.org/10.1088/0022-3727/41/13/135103>.
- Güllü, Ö., Demir, F., Cimilli, F.E., Biber, M., 2008b.  $\gamma$ -Irradiation-induced changes at the electrical characteristics of Sn/p-Si Schottky contacts. *Vacuum* 82, 789–793. <https://doi.org/10.1016/j.vacuum.2007.11.006>.
- Kaya, S., Aktag, A., Yilmaz, E., 2014. Effects of gamma-ray irradiation on interface states and series-resistance characteristics of BiFeO<sub>3</sub> MOS capacitors. *Nucl. Instruments Methods Phys. Res. Sect. B Beam Interact. with Mater. Atoms* 319, 44–47. <https://doi.org/10.1016/j.nimb.2013.11.006>.
- Kaymaz, A., Uslu Tecimer, H., Evcin Baydilli, E., Altindal, S., 2020. Investigation of gamma-irradiation effects on electrical characteristics of Al/(ZnO-PVA)/p-Si Schottky diodes using capacitance and conductance measurements. *J. Mater. Sci. Mater. Electron.* 31, 8349–8358. <https://doi.org/10.1007/s10854-020-03370-2>.
- Khanna, R., Ip, K., Allums, K.K., Baik, K., Abernathy, C.R., Pearton, S.J., Heo, Y.W., Norton, D.P., Ren, F., Shojah-Ardalan, S., Wilkins, R., 2005. Proton irradiation of ZnO Schottky diodes. *J. Electron. Mater.* 34, 395–398. <https://doi.org/10.1007/s11664-005-0117-2>.
- Kumar, M.V., Kumar, S., Cheng, C., Asokan, K., Kumar, A., Shobha, V., Karanth, S.P., Krishnaveni, S., 2017. Influence of high dose gamma irradiation on electrical characteristics of Si photo detectors. *ECS J. Solid State Sci. Technol.* 6, 132–135. <https://doi.org/10.1149/2.011710jss>.
- Laha, P., Banerjee, I., Barhai, P.K., Das, A.K., Bhoraskar, V.N., Mahapatra, S.K., 2012. Effects of 6 MeV electron irradiation on the electrical properties and device parameters of Al/Al<sub>2</sub>O<sub>3</sub>/TiO<sub>2</sub>/n-Si MOS capacitors. *Nucl. Instruments Methods Phys. Res. Sect. B Beam Interact. with Mater. Atoms* 283, 9–14. <https://doi.org/10.1016/j.nimb.2012.04.014>.
- Mamor, M., Sellai, A., Bouziane, K., Al Harthi, S.H., Al Busaidi, M., Gard, F.S., 2007. Influence of He-ion irradiation on the characteristics of Pd/n-Si/0.90Ge0.10/Si Schottky contacts. *J. Phys. D Appl. Phys.* 40, 1351–1356. <https://doi.org/10.1088/0022-3727/40/5/007>.
- Matoussi, A., Boufaden, T., Guermazi, S., Mlik, Y., El Jani, B., Toureille, A., 2005. Electron beam-induced current investigation of GaN Schottky diode. *J. Electron. Mater.* 34, 1059–1064. <https://doi.org/10.1007/s11664-005-0096-3>.
- Maurya, S., Awasthi, S., 2018. Effect of zero bias, 2.7 MeV proton irradiation on HfO<sub>2</sub>. J. Radioanal. Nucl. Chem. 318, 947–953. <https://doi.org/10.1007/s10967-018-6229-y>.
- Nezhadesm-Kohardafchahi, S., Farjam-Shayesteh, S., Badali, Y., Altindal, Jamshidi-Gholzlu, M.A., Azizian-Kalandaragh, Y., 2018. Formation of ZnO nanopowders by the simple ultrasound-assisted method: exploring the dielectric and electric properties of the Au/(ZnO-PVA)/n-Si structure. *Mater. Sci. Semicond. Process.* 86, 173–180. <https://doi.org/10.1016/j.mssp.2018.06.030>.
- Nicollian, E.H., Brews, J.R., 2003. *MOS (Metal Oxide Semiconductor) Physics and Technology*. Wiley, Hoboken, NJ, USA.
- Norde, H., 1979. A modified forward I-V plot for Schottky diodes with high series resistance. *J. Appl. Phys.* 50, 5052–5053. <https://doi.org/10.1063/1.325607>.
- Orak, I., Kocigit, A., Alindal, S., 2017. Electrical and dielectric characterization of Au/ZnO/n-Si device depending frequency and voltage. *Chin. Phys. B* 26. <https://doi.org/10.1088/1674-1056/26/2/028102>.
- Paradzah, A.T., Omotoso, E., Legodi, M.J., Auret, F.D., Meyer, W.E., Diale, M., 2016. Electrical characterization of high energy electron irradiated Ni/4H-SiC Schottky barrier diodes. *J. Electron. Mater.* 45, 4177–4182. <https://doi.org/10.1007/s11664-016-4609-z>.
- Reddy, V.R., 2014. Electrical properties of Au/polyvinylidene fluoride/n-InP Schottky diode with polymer interlayer. *Thin Solid Films* 556, 300–306. <https://doi.org/10.1016/j.tsf.2014.01.036>.
- Rhoderick, E.H., Williams, R.H., 1988. *Metal-Semiconductor Contacts*, second ed. Clarendon Press, Oxford.
- Sahin, R., Kabacelik, I., 2018. Effects of ionizing radiation on the properties of monocrystalline Si solar cells. *Radiat. Phys. Chem.* 150, 90–94. <https://doi.org/10.1016/j.radphyschem.2018.04.033>.
- Sekhar Reddy, P.R., Janardhanam, V., Jyothi, I., Yuk, S.H., Rajagopal Reddy, V., Jeong, J.C., Lee, S.N., Choi, C.J., 2016. Modification of Schottky barrier properties of Ti/p-type InP Schottky diode by polyaniline (PANI) organic interlayer. *J. Semicond. Technol. Sci.* 16, 664–674. <https://doi.org/10.5573/JSTS.2016.16.5.664>.
- Srour, J.R., Marshall, C.J., Marshall, P.W., 2003. Review of displacement damage effects in silicon devices. *IEEE Trans. Nucl. Sci.* 50, 653–670.
- Srour, J.R., Palko, J.W., 2013. Displacement damage effects in irradiated semiconductor devices. *IEEE Trans. Nucl. Sci.* 60, 1740–1766. <https://doi.org/10.1109/TNS.2013.2261316>.
- Sze, S.M., Ng, K.K., 2006. *Physics of Semiconductor Devices*, third ed. Physics of Semiconductor Devices. John Wiley & Sons, Inc., Hoboken, NJ, USA <https://doi.org/10.1002/0470068329>.
- Taşçıoğlu, I., Tüzün Özmen, Şağban, H.M., Yağlıoğlu, E., Altindal, 2017. Frequency dependent electrical and dielectric properties of Au/P3HT: PCBM:F4-TCNQ/n-Si Schottky barrier diode. *J. Electron. Mater.* 46, 2379–2386. <https://doi.org/10.1007/s11664-017-5294-2>.
- Tataroğlu, A., Altindal, S., 2007. Analysis of interface states and series resistance at MIS structure irradiated under 60Co  $\gamma$ -rays. *Nucl. Instruments Methods Phys. Res. Sect. A Accel. Spectrometers., Detect. Assoc. Equip.* 580, 1588–1593. <https://doi.org/10.1016/j.nima.2007.07.027>.
- Tataroğlu, A., Altindal, S., Bölküdemir, M.H., Tanır, G., 2007. Irradiation effect on dielectric properties and electrical conductivity of Au/SiO<sub>2</sub>/n-Si (MOS) structures. *Nucl. Instruments Methods Phys. Res. Sect. B Beam Interact. with Mater. Atoms* 264, 73–78. <https://doi.org/10.1016/j.nimb.2007.07.026>.
- Teffahi, A., Hamri, D., Mostefa, A., Saidane, A., Al Saqr, N., Felix, J.F., Henini, M., 2016. Effect of 60Co  $\gamma$ -ray irradiation on electrical properties of Ti/Au/GaAs<sub>1-x</sub>N Schottky diodes. *Curr. Appl. Phys.* 16, 850–858. <https://doi.org/10.1016/j.cap.2016.05.003>.

- Tian, J., Cao, G., 2016. Design, fabrication and modification of metal oxide semiconductor for improving conversion efficiency of excitonic solar cells. *Coord. Chem. Rev.* 320–321, 193–215. <https://doi.org/10.1016/j.ccr.2016.02.016>.
- Tobnaghi, D.M., Rahnamaei, A., Vajdi, M., 2014. Experimental study of gamma radiation effects on the electrical characteristics of silicon solar cells. *Int. J. Electrochem. Sci.* 9, 2824–2831.
- Tüzün, Ö., Altindal, Ş., Oktik, Ş., 2008. Effects of illumination and 60Co  $\gamma$ -ray irradiation on the electrical characteristics of porous silicon solar cells. *Renew. Energy* 33, 286–292. <https://doi.org/10.1016/j.renene.2007.05.019>.
- Uslu, H., Yıldırım, M., Altindal, Ş., Durmuş, P., 2012. The effect of gamma irradiation on electrical and dielectric properties of organic-based Schottky barrier diodes (SBDs) at room temperature. *Radiat. Phys. Chem.* 81, 362–369. <https://doi.org/10.1016/j.radphyschem.2011.12.029>.
- Verma, S., Praveen, K.C., Bobby, A., Kanjilal, D., 2014. Recovery of electrical characteristics of Au/n-Si Schottky junction under 60Co gamma irradiation. *IEEE Trans. Device Mater. Reliab* 14, 721–725. <https://doi.org/10.1109/TDMR.2014.2312753>.
- Vijayalakshmi, S., Venkataraj, S., Jayavel, R., 2008. Characterization of cadmium doped zinc oxide (Cd : ZnO) thin films prepared by spray pyrolysis method. *J. Phys. D Appl. Phys.* 41 (245403) <https://doi.org/10.1088/0022-3727/41/24/245403>.
- Winokur, P.S., Schwank, J.R., McWhorter, P.J., Turpin, D.C., Dressendorfer, P.V., 1984. Correlating the radiation response of mos capacitors and transistors. *IEEE Trans. Nucl. Sci.* 31, 1453–1460. <https://doi.org/10.1109/TNS.1984.4333529>.
- Xu, Y., Bi, J., Xi, K., Liu, M., 2019. The effects of  $\gamma$ -ray irradiation on graphene/n-Si Schottky diodes. *APEX* 12. <https://doi.org/10.7567/1882-0786/able98>, 061004.